Case Studies in Construction Materials 15 (2021) e00552

Contents lists available at ScienceDirect

Case Studies in Construction Materials

journal homepage: www.elsevier.com/locate/cscm

Case study

Experimental and numerical analysis on the effectiveness of GFRP wrapping system on timber pile rehabilitation

Weena Lokuge[a,*], Omar Otoom[b], Rahmin Borzou[c], Satheeskumar Navaratnam[d], Nilupa Herath[e], David Thambiratnam[f]

[a] Centre for Future Materials, School of Civil Engineering and Surveying, University of Southern Queensland, Springfield Campus, QLD, 4300, Australia
[b] Centre for Future Materials, School of Civil Engineering and Surveying, University of Southern Queensland, Springfield Campus, QLD, 4300, Australia
[c] QuakeWrap-Australia, Tennyson, QLD, 4105, Australia
[d] School of Engineering, RMIT University, Australia
[e] Department of Infrastructure Engineering, University of Melbourne, VIC, 3001, Australia
[f] School of Civil and Environmental Engineering, Queensland University of Technology, Brisbane, QLD, 4001, Australia

ARTICLE INFO

Article history:
Received 10 February 2021
Received in revised form 26 March 2021
Accepted 15 April 2021

Keywords:
Timber column
GFRP wrapping system
Splitting
Infill material
Axial load capacity
Ductility
Energy absorption

ABSTRACT

Rehabilitation using Glass Fibre Reinforced Polymer (GFRP) wrapping system is an innovative technique for rehabilitation of deteriorated timber structures exposed to severe environmental conditions. This paper investigates the effectiveness of rehabilitation using GFRP wrapping system for deteriorated timber piles due to splitting. An experimental investigation was conducted on undamaged and damaged short timber columns with three levels of splitting. Crane rail epoxy and underwater cementitious grout were used to fill the annulus between columns and GFRP jackets in the rehabilitated samples. All the samples were tested under axial compression loading. Axial peak and yield loads, ductility and energy absorption were discussed to assess the overall behaviour of timber columns. In addition, a finite element analysis was established to investigate the overall load-deformation performance of the tested samples and to validate the experimental results. Furthermore, an analytical prediction was performed based on Australian Standards along with an existing GFRP wrapped stress- strain model to determine the peak load capacity of the unwrapped and GFRP wrapped samples. The experimental results indicated that the GFRP wrapping system can restore the axial capacity and energy absorption of the damaged samples with high effectiveness was observed for samples infilled by the crane rail epoxy. Also, the results of numerical and analytical analysis showed a reasonable correlation with the experimental results.

1. Introduction

The aging timber bridge stock around the world creates a strong financial commitment to the road authorities. The maintenance cost of timber bridges is relatively high and is affected significantly by several deterioration mechanisms, which require a systematic approach for diagnosis and treatment [1]. The approaches used to rehabilitate timber bridges

* Corresponding author.
E-mail address: weena.lokuge@usq.edu.au (W. Lokuge).

https://doi.org/10.1016/j.cscm.2021.e00552

vary depending on the timber deterioration mechanism, the type of structural member and the location. This requires a dire need of finding cost effective and structurally efficient rehabilitation methods which can prolong the service life of the timber bridges.

Current timber bridge stock in Australian roads is definitely having timber piles as primary structural support. Timber pile deterioration initiates and spreads due to many reasons such as wetting and drying cycles, which result in timber shrinkage and involve large internal stresses. Moisture existence causes thermal expansion to occur and when wood is unprotected from external factors; moisture can be absorbed in both the cell walls and the cell cavities. The result of this is cracking along the fibres, opening the timber for fungal decay to start breeding. Termites is another means that a pile can deteriorate rapidly and damage caused by termites is a quicker process than that of fungi [2]. It is less common to see termite attack in durable hardwoods without any pre-existing fungal decay. This is due to the fact that moisture presence provides excellent environment for termite growth [3]. In addition, timber piles that are submerged beneath the water surface can be inhabited by marine organisms which becomes more severe in subtropical waters than in colder waters [4]. Splitting is another factor in reducing the strength of timber pile and is defined as separation along the grain extending right through the member and it is caused by thermal expansion, fluctuations of moisture content and overloading [5]. Queensland timber bridge maintenance manual [6] stipulates that cracks may be aggravated by overloading and vehicular collision which cause splitting to start from the bearing area and travels upwards to the timber girder.

Prediction of the failure of timber bridges has been studied in the past [7]. Various techniques have been used to rehabilitate the timber bridges such as cutting and posting which is performed by simply cutting the deteriorated sections of a pile and then replacing by a new timber segment using steel pins or nails or epoxy-grouted to produce a permanent bond between the two sections [8]. Another repair technique is injecting cementitious grout into the voids of a decayed timber through drilled holes and this technique was mainly used to prevent the decay extension to other sections [9]. Concrete jacketing is an alternative rehabilitating technique for deteriorated timber piles where a steel cage is placed around affected area of the existing timber pile and then concrete jackets are formed using 25–50 mm thick coat. This method has its downfall as concrete is likely to be subjected to external factors such as acids, alkaline or salt in ground water which may cause drastic effects such as cracking and spalling [2]. This will eventually cause exposure of the steel cage and result in corrosion and loss of cross-sectional area, strength and durability. Austroads [5] suggests concrete jacketing as a repair method and does not provide details about how the repair should be carried out or implemented. On the other hand, rehabilitation using steel plates or fibre composites has also proven their high contribution to stiffness and ductility of timber columns [10,11] and offer a protection from biological attack for submerged timber pile [12].

In recent decades, retrofitting by fibre reinforced polymer (FRP) wrapping systems has become popular [13–15]. The FRP wrapping systems can be easily installed on site without a need for heavy machinery and it has been investigated to be the best method of rehabilitating timber piles [16–18]. The FRP wrap and the surrounding grout shell completes the retrofit and it is capability to restore axial strengths with minimal reduction in stiffness [19]. Lopez-Anido, et al. [20] investigated the performance of timber piles using two types of load-transfer mechanisms, cement-based structural grout and the steel shear connectors with an expanding polyurethane chemical grout. They studied the response of pre-damaged timber piles repaired with the FRP composite shield system under the effect of flexural loading. The results indicated that the FRP composite shield with cement-based grouting system restored the bending capacity and exceeded the capacity of the reference undamaged sample. Gull, et al. [16] also carried out tests on five full-scale timber pile specimens with different levels of damages, wherein GFRP jackets with fibers oriented in two perpendicular directions were used to rehabilitate the specimens using different filling materials. Their study results showed that the used GFRP wrapping system restored the designed load capacity and failed at higher loads. The study, however, showed the effectiveness of pile repair by GFRP laminates wrapped around the damaged regions with annulus infilled by grout or epoxy. Ghazijahani, et al. [21] studied the compression performance of different shapes and geometries of timber cores surrounded by concrete and encased in steel tubes. The results indicated that the used composite system enhanced the capacity, ductility and energy absorption. An experimental study carried out by Raongjant and Meng [22] presented the effect of two different FRP strengthening techniques on the performance of damaged hardwood timber columns under uniaxial and biaxial eccentric compression. The damage was initiated by split cuts of 2 mm width along the tested specimens. The depth of these splits varied between 30 mm and 60 mm to simulate 25 % and 50 % damages, respectively. The results indicated that the damage size had a significant effect on the bearing capacity of columns under compression. However, the FRP strengthening was found to have a substantial contribution to the capacity of all columns. Furthermore, Wei et al. [23] indicated that longitudinal splitting failure was one of the main failure modes experienced by cross-laminated timber and glued-laminated timber columns. Therefore, splitting damage is an essential deteriorating parameter than can affect the performance of timber columns and has to be further investigated. From the previous studies, it is evident that rehabilitation of timber piles is a necessity in maintaining their structural integrity. Also, a gap in knowledge has been noted with split depth not incorporated into the bridge maintenance and inspection guidelines or tested for reduction in axial strength.

Lateral confinement of FRP jackets significantly enhances the strength and ductility of existing structure and it must be sufficiently stiff to develop appropriate confining forces at relatively low axial strain levels [24,25]. The gain in compressive strength obtained by the Carbon FRP confined concrete depended mainly on the relative stiffness of the FRP jacket to the axial stiffness of the column [25]. Many studies considered variable parameters and their effect on the performance of wrapped columns [15,26–29]. Moreover, several models were developed for the confining pressure of FRP jackets [27,30–

37]. A review by Ozbakkaloglu, et al. [38] stated that the models developed by [31,39] can be classified as the most accurate FRP-confined stress-strain model in predicting the peak stresses and strains. Although, several studies have considered the confinement effectiveness on concrete columns, limited research has been conducted to investigate the behaviour of timber columns as well as the effect of infill materials.

Identifying and developing an appropriate rehabilitation technique with high strength, cost effective and flexible in term of installation, will reduce the maintenance cost of infrastructure industries. Thus, this research aims to develop an effective retrofitting technique using GFRP wrapping system. The experimental results for timber columns with splits under axial compression have been presented. The innovated technique of using GFRP laminates with two different infill materials has been found to be effective in increasing the peak and yield loads, deformations and ductility of the deficient timber columns. In addition, this study has presented a finite element model (FEM) using ABAQUS [40] and the model was validated with the experimental results. Furthermore, an analytical prediction for the peak load capacity of the GFRP wrapped timber columns was conducted by considering the contribution of the timber section and the GFRP jacket. These predictions will be compared and verified with the experimental results.

2. Research significance

Splitting depth is not considered as a criteria in the bridge maintenance and inspection guidelines [3] or it is not been tested for reduction in axial strength. This research focuses on repairing deteriorated timber piles using GFRP wrapping system. The underwater cementitious grout (CM) [41] and crane rail epoxy (CR) [42] were selected as the infill materials for the annulus between GFRP jackets and the base timber columns. These materials offer a high degree of confinement, increase strength, and maintain performance of the retrofitted piles. It is important to understand the effectiveness of the GFRP wrapping system in rehabilitating the deteriorated timber piles which will lead to a broad utilisation of such techniques. Thus, adopting this assessment will provide a foundation for further development and research into this technique.

3. Experimental program

This research focuses on investigating the effect of a GFRP wrapping system in rehabilitating the timber piles deteriorated due to splitting. The experimental program included testing of 16 short cylindrical timber columns (Grade F27 timber) under axial compression loading. All base timber samples had an approximate diameter of 200 mm and a height of 300 mm. In this study, the testing variables include the effect of three damage levels (1/3, 2/3 and full radius splitting along the longitudinal direction of the column) and the effect of varying the infill materials.

Table 1 lists the details of all tested samples which included four unwrapped control samples; one undamaged and three damaged samples. Six damaged samples (including duplicates) were wrapped with GFRP laminates with around 20 mm annulus infilled by CM grout and six other damaged samples (including duplicates) were wrapped with GFRP laminates with around 20 mm annulus infilled by CR epoxy. Duplicating samples was adopted to ensure the accuracy of results and also to be used for future developments. The testing of samples was carried out after 28 days of casting.

The samples were labelled using the following configuration: the first letter indicates the wrapping condition where W and U refer to wrapped and unwrapped samples, respectively. The second letter or number refers to the degree of splitting damage introduced in the samples where F, 2/3 and 1/3 refer to the defects of full, two-third and one third radius, respectively. In addition, the number zero refers to undamaged sample. Finally, the last letters represents the used infill where CM and CR refer to the underwater cementitious and crane rail epoxy, respectively and numbers 1and 2 refer to the duplicate samples. For instance, the sample W-2/3-CM-2 refers to the second wrapped sample with 2/3 radius splitting and annulus infilled by underwater cementitious grout and sample U-0 refers to the unwrapped control sample with no damage.

Table 1
Details of samples.

Sample	Damage	GFRP wrapping	Infill
W-F-CM-1,2	Full radius	Wrapped	CM
W-F-CR-1,2	Full radius	Wrapped	CR
U-F	Full radius	–	–
W-2/3-CM-1,2	2/3 radius	Wrapped	CM
W-2/3-CR-1,2	2/3 radius	Wrapped	CR
U-2/3	2/3 radius	–	–
W-1/3-CM-1,2	1/3 radius	Wrapped	CM
W-1/3-CR-1,2	1/3 radius	Wrapped	CR
U-1/3	1/3 radius	–	–
U-0	No damage	–	–

Table 2
Materials properties.

Material	Strength (MPa)	Modulus of elasticity (GPa)	Thickness (mm)
F27 timber	51 (compression) 67 (flexural) 42 (tension)	18.5	≈ 200
Cementitious grout	48.3 (compression)		20
Crane rail epoxy	108 (compression)	15.9	20
GFRP laminate	431(tension-Longitudinal) 418 (tension-transverse)	24.14 – 25.25	2.05
Underwater Resin 220UR	38.6 (tension)	23.4–26.2	2

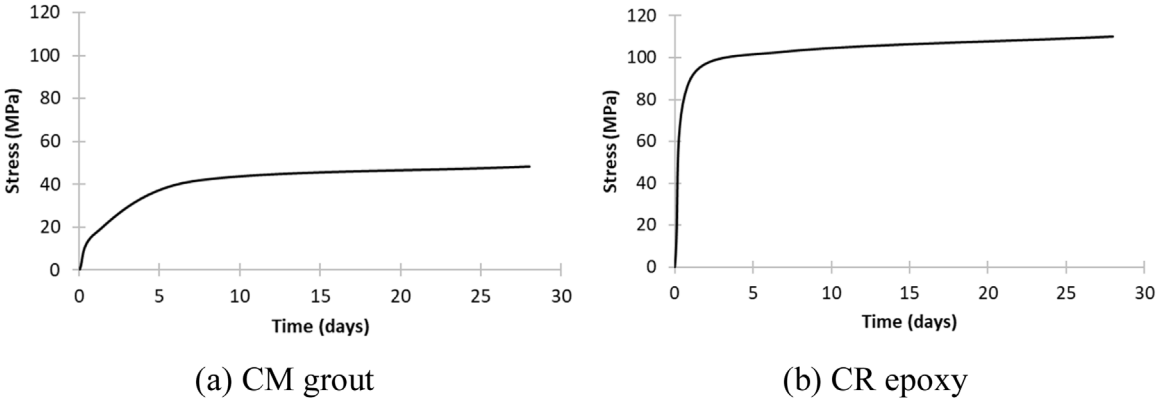

Fig. 1. Strength development of grout and epoxy infills.

3.1. Properties of materials

Table 2 lists the properties of the various materials used in this testing program. The F27 timber samples were sourced through the University of Southern Queensland and properties of this timber were based on the data provided by AS 1720.1–2010 [43]. The infill materials and GFRP laminates were supplied by QuakeWrap,Inc. Australia [44].

PileMedic^{TM} PLG60.60 [45] is the GFRP laminate used to wrap the samples in this study. This laminate is characterized by providing high strength in axial and transverse directions as it contains bidirectional glass fibres equally distributed in both directions. Fig. 1 shows the strength development of the infill materials over the first 28 days whereas, CM grout (Fig. 1a) achieved a peak stress of 48.3 MPa compared to 108 MPa achieved by CR epoxy (Fig. 1b).

The selection of infill materials was based on their high strength properties, pumpability and workability. Test results of the CM and CR infills revealed that 90 % of their compressive strength was achieved after 7 days.

3.2. Preparation of testing samples

The preparation of testing samples is described in Fig. 2. The GFRP jackets were cast using two laminates glued together (Fig. 2a) with QuakBond ^{TM} 220 UR resin [46] whereas the longitudinal direction of fibres was oriented in the hoop direction of the cylinders. The infill materials were mixed and prepared as described in the technical data sheets [41,42]. After that, the timber columns were properly placed, centralized and clamped inside the jackets using annular spacers of 20 mm (Fig. 2b and c) to maintain the desired gap for the infills. Finally, the infills were poured in the annulus gap (Fig. 2 ande)

3.3. Damage levels

A severe vertical split would be greater than 5 mm in width and extending more than a meter in length and the splits may be wider than 5 mm but have shorter length or vice versa [3]. This was the only information available from road authorities about splitting measurements. Splitting was introduced into all samples except the undamaged control sample. The splitting used in this research runs along the entire height of the sample (approximately 300 mm) with various depths of full radius, 2/3 radius and 1/3 radius as shown in Fig. 3. Even though the split damages in real-life timber columns are random and cannot be controlled, the proposed damaging technique can be relatively representative. According to previous studies [23,47,48], the longitudinal sudden splitting failure in timber fibres was the dominant failure mode of timber columns under

(a) Resin application (b) Annular spacers (c) GFRP wrap

(d) A sample with CM infill (f) A sample with CR infill

Fig. 2. Preparation of samples.

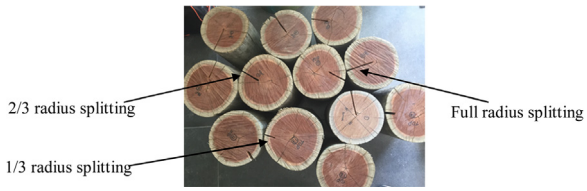

Fig. 3. Split defects.

compression. In addition, the split depths can vary in a wide range from 12.5 % up to 50 % of the section width [49], thus the splitting damages used herein can approximately simulate the actual deterioration of timber columns in actual practices.

3.4. Instrumentation and test procedure

The compression tests of the unwrapped samples were carried out using SANS compression testing machine with a capacity of 2000 kN (Fig. 4a). Compression load was applied through displacement control at 2 mm /min. Due to the limitation in the capacity of the SANS testing machine, a universal testing machine with a capacity of 5000 kN (Fig. 4b) was also used in this testing program to test the wrapped samples. The axial loads and deformations were obtained from the computer system of the testing machines.

3.5. Definition of strengthening ratio, ductility and energy absorption

To study the influence of the rehabilitation method, the strengthening ratios at both yield and peak load were calculated. The yield strengthening ratio is defined as the ratio between the yield load of the tested sample and the yield load of corresponding control sample. The peak strengthening ratio is defined as the ratio between the peak load of the tested sample and the peak load of corresponding control sample [50]. Energy absorption was determined as the area under the load-deformation curve until failure and energy absorption ratio was determined by dividing the energy absorption of the tested sample by the energy absorption of the corresponding control sample [50]. The ductility factor of tested samples was calculated by dividing the deformation of the tested sample at failure load by the deformation at yield load. The deformation

Fig. 4. Compression test setup.

at yield was determined as described by Jorissen and Fragiacomo [51] by multiplying the deformation at 40 % of the peak load by 1.25 and then the yield load was determined as the relevant load to the deformation at yield.

4. Results and discussions

4.1. Behaviour of control samples

Fig. 5 shows the load-deformation curves for the unwrapped samples including the undamaged, full radius damaged, 2/3 radius damaged and 1/3 radius damaged. This figure illustrates that the induced damages have reduced the axial capacity of the columns. The red circles in Fig. 5 show the crack initiation during loading of specimens.

The load-deformation curves show that all samples exhibited similar initial response until approximately 70 % of the peak load. Afterwards, a descending response was observed by the defected samples up to the peak load. However, sample U-2/3 showed a lower stiffness compared to other samples. This indicates that defects in columns can definitely affect the overall behaviour of timber columns. Table 3 summarizes the experimental results for the unwrapped control samples. Sample U-1/3 had the smallest incorporated defect and results showed that it had the lowest axial yield and axial peak load capacities among all control samples and also, the energy absorption was lower than other defected samples. Unfortunately, this timber member had a knot close to the ends, which resulted in exhibiting a lower axial capacity and weakening in the lateral direction. It was observed that a split through the decayed knot along the grain with approximately 15 mm in width started to extend in the longitudinal direction as shown in Fig. 5. Gilfillan et al. [52] indicated that the strength capacity of timber structures is significantly reduced due to the presence of knots and other distortions in the grain. This effect is however more influencing for structures under tension than compression or bending. The unforeseen flaws in natural timber such as the knots in this experiments will be taken into consideration during the design process by considering the capacity reduction factors. Even though, specimen U-2/3 showed a slightly reduced stiffness compared to other control samples, it achieved the highest peak load capacity among the defected samples with highest energy absorption ratio. This energy absorption was 171 % higher than the energy absorption of control undamaged sample and this was due to experiencing high deformation at failure. In addition, U-2/3 sample demonstrated higher yield strength and peak strength ratios compared to U-F. This indicates that the degree of splitting damage greatly influences the axial load-deformation behaviour. This influence can also be observed in the loads at failure, as the axial load dropped by 18 % and 31 % for samples U-F and U-2/3, respectively. Nevertheless, samples U-F and U-2/3 showed approximately similar ductility.

The failure of all defected samples was governed by timber crushing near the top ends which propagated to the other locations of the column until failure. However, the control undamaged sample U-0 showed only formation of cracks and no failure was noticed with the graph kept climbing before the loading machine stopped logging results. Sample U-0 had the lowest ductility and lowest energy absorption and this was due to not exhibiting a post peak response. The sample U-0 achieved a peak load of 1800 kN with corresponding peak stress of 59.32 MPa.

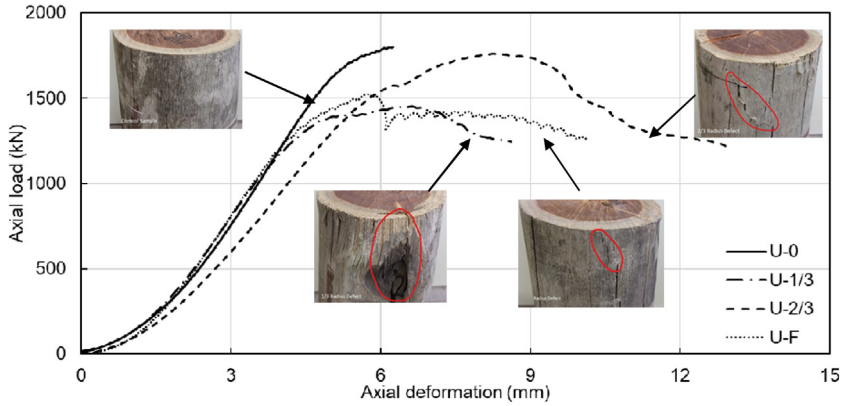

Fig. 5. Axial load-deformation curves of control samples.

Table 3
Experimental results of control samples.

Sample	U-F	U-2/3	U-1/3	U-0
Yield axial load (kN)	884	998	837	1043
Peak axial load (kN)	1523	1760	1451	1800
Axial load at failure (kN)	1254	1209	1243	1800
Axial deformation at yield load (mm)	3.16	4.13	3.08	3.63
Axial deformation at peak load (mm)	5.74	8.24	6.62	6.24
Axial deformation at failure load (mm)	10.12	13.03	8.6	6.24
Energy Absorption (kN-mm)	10366	14721	8181	5427
Ductility factor	3.20	3.15	2.79	1.72
Energy Absorption ratio	1.91	2.71	1.51	1.00
Yield strengthening ratio	0.85	0.96	0.80	1.00
Peak strengthening ratio	0.85	0.98	0.81	1.00

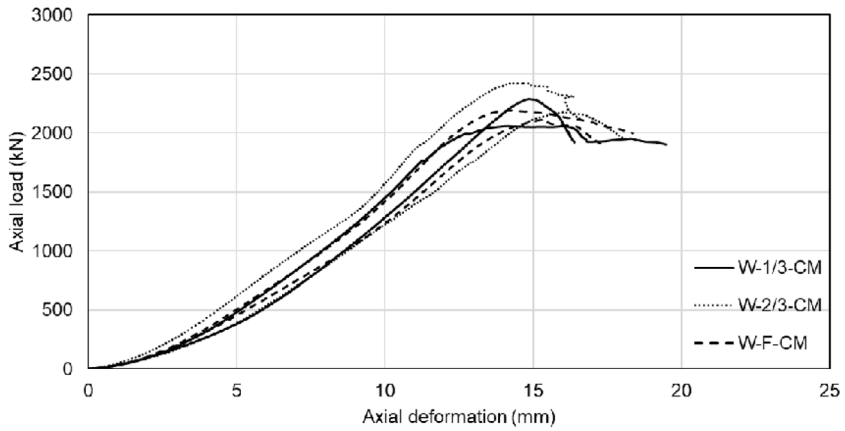

Fig. 6. Axial load-deformation curves of samples infilled with CM grout.

4.2. Behaviour of samples wrapped with GFRP and infilled by CM grout

Fig. 6 depicts the axial load–deformation curves for samples wrapped by GFRP jackets with annulus infilled by CM grout. All samples in this group exhibited higher yield and peak strength ratios compared to the defected control samples and this indicates the effectiveness of GFRP wrapping confinement. The yield loads of wrapped defected samples exceed the yield loads of control defected samples with the highest average of 49 % observed in W-1/3-CM samples. The peak axial load capacities were increased by an average of 41 %, 31 % and 50 % for W-F-CM, W-2/3-CM, W-1/3-CM samples, respectively. In general, all wrapped samples with annulus infilled by CM grout showed a significant increase in energy absorption compared to the control unwrapped samples. This is due to exhibiting high deformations at yield and also achieving high peak loads.

Fig. 7. Failure modes of samples infilled with CM grout.

Table 4
Experimental results of wrapped samples infilled with CM grout.

Sample	W-F-CM-1	W-F-CM-2	W-2/3-CM-1	W-2/3-CM-2	W-1/3-CM-1	W-1/3-CM-2
Yield axial load (kN)	1161	1213	1225	1158	1336	1158
Peak axial load (kN)	2116	2191	2176	2428	2289	2059
Axial load at failure (kN)	1881	1998	1947	2100	1920	1902
Axial deformation at yield load (mm)	9.6	9.0	10.0	12.4	10.2	8.7
Axial deformation at peak load (mm)	15.4	14.3	16.0	14.3	14.9	14.1
Axial deformation at failure load (mm)	17.5	18.4	18.2	16.7	16.4	19.5
Energy Absorption(kN-mm)	18637	22387	19705	21115	16902	23883
Ductility factor	1.82	2.04	1.82	1.35	1.61	2.25
Yield strengthening ratio	1.31	1.37	1.23	1.16	1.60	1.38
Peak strengthening ratio	1.39	1.44	1.24	1.38	1.58	1.42
Energy Absorption ratio	1.80	2.16	1.34	1.43	2.07	2.92

Furthermore, all samples with CM grout infills performed similarly in the pre peak response whilst the post peak response showed a rapid descending response.

The failure of specimens W-F-CM1 and W-F-CM2 (Fig. 7a) started by formation of cracks at the sample top third region. These cracks started to propagate and widen in the circumferential direction due to lateral dilation until failure occurred due to GFRP rupture. Moreover, samples W-2/3-CM-1 and W-2/3-CM-2 had a similar failure to samples with full radius defect. However, the final failure was followed by the separation of the laminates along the overlapped region as shown in Fig. 7b. The failure of the samples with 1/3 radius defect showed similarity with that of the samples with full radius defect (Fig. 7c).

Sample W-2/3-CM2 exhibited the highest load carrying capacity of 2428 kN whilst sample W-1/3-CM2 had the lowest peak load and lowest axial deformation at peak as shown in Table 4. This indicates that the degree of split defect in timber columns can significantly affect the ability of structure to sustain high deformations. It is apparent that the confinement by GFRP laminates with annulus infilled with CM grout has a significant effect on axial load capacities and energy absorption. Based on the experimental results presented so far, it can be seen that cementitious grout was very effective in enhancing the overall compression performance and also in repairing piles with splitting irrespective of the damage level.

4.3. Behaviour of samples wrapped with GFRP and infilled by CR epoxy

The confinement provided by GFRP wrapping maintains higher yield, peak strength and energy absorption ratios compared to the unwrapped samples. The highest increase in yield and peak strengthening ratios was reported to be 238 % and 214 %, respectively in W-1/3-CR-2. The axial load–deformation curves for samples strengthened by GFRP laminates with annulus infilled by CR epoxy are shown in Fig. 8. It is well observed that samples with full radius defect exhibited a significant reduction in peak axial loads and corresponding deformations. As summarized in Table 5, energy absorption of GFRP wrapped sample with CR epoxy significantly increased with an average of 114 %, 107 % and 263 % in full radius, 2/3 radius and 1/3 radius defect, respectively compared to unwrapped samples. This indicates that crane rail epoxy has an apparent contribution to the energy absorption of all samples with various defects. An average increase in the axial yield load was noticed in the wrapped samples to 80 %, 46 % and 144 % in the full radius, 2/3 radius and 1/3 radius defect samples,

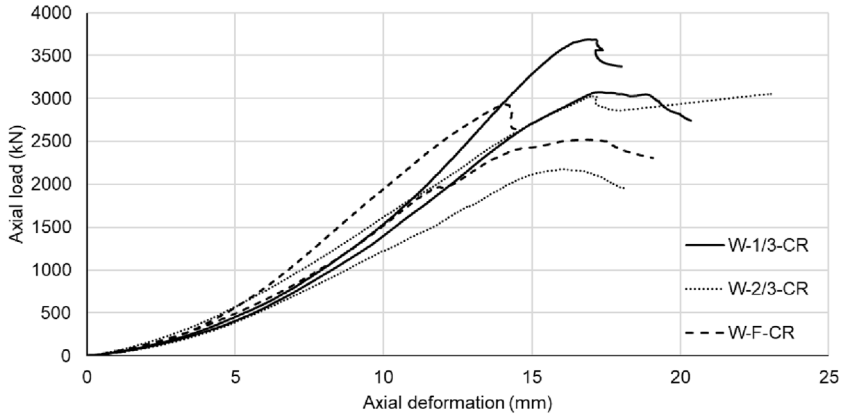

Fig. 8. Axial load-deformation curves of samples infilled with CR grout.

Table 5
Experimental results of wrapped samples infilled with CR epoxy.

Sample	W-F-CR-1	W-F-CR-2	W-2/3-CR-1	W-2/3-CR-2	W-1/3-CR-1	W-1/3-CR-2
Yield Axial load (kN)	1719	1472	1224	1683	1827	2264
Peak axial load (kN)	2933	2520	2177	3033	3074	3689
Axial load at failure (kN)	2641	2307	1947	3045	2742	3374
Axial deformation at yield load (mm)	9.2	9.8	10.0	10.3	11.6	12.2
Axial deformation at peak load (mm)	14.1	16.8	16.0	17.0	17.3	16.9
Axial deformation at failure load (mm)	14.5	19.1	18.1	23.1	20.4	18.0
Energy Absorption(kN-mm)	18306	26010	19705	41232	31184	28118
Ductility factor	1.57	1.94	1.81	2.25	1.75	1.47
Yield strengthening ratio	1.94	1.67	1.23	1.69	2.18	2.70
Peak strengthening ratio	1.92	1.65	1.24	1.72	2.11	2.54
Energy Absorption ratio	1.77	2.51	1.34	2.80	3.81	3.44

Fig. 9. Failure modes in samples infilled with CR epoxy.

respectively. Highest ductility factor was noticed for sample W-2/3-CR2 and this is due to experiencing high deformation. However, ductility factor slightly reduced if compared with samples infilled by CM grouts and this could be attributed to the increase in brittleness of the epoxy infills due to the strength increase.

The failure of full radius, 2/3 radius defect and 1/3 radius defect samples (Fig. 9a–c) started by appearance of circumferential cracks near the top part of the tested cylinders followed by rapid propagation through the GFRP before final failure occurred by GFRP rupture. However, the failure of samples with 2/3 radius defect was accompanied with separation of the GFRP laminates over the overlapped region.

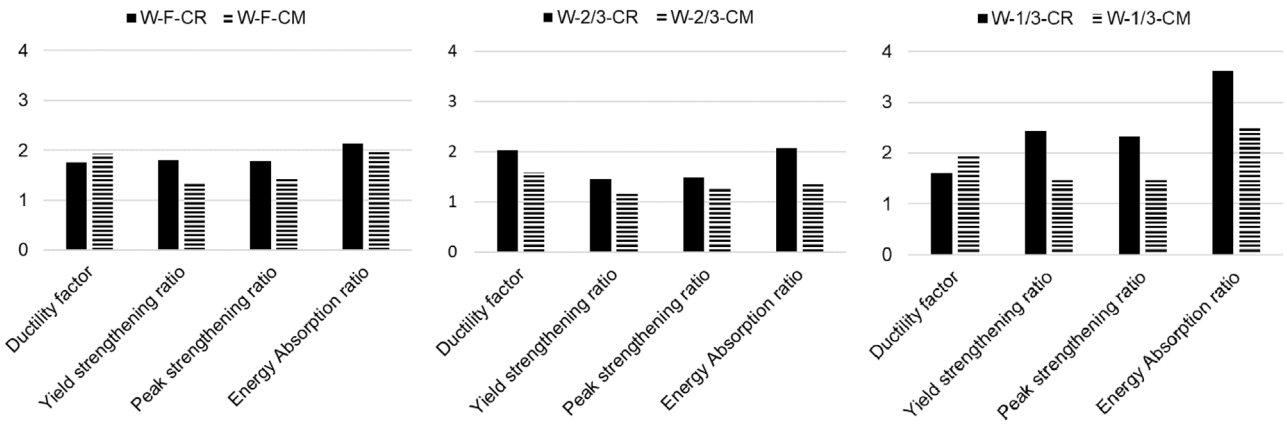

Fig. 10. Comparison between CM and CR infills.

Fig. 10 depicts a comparison between CM and CR infills and their effect on ductility factor, yield strengthening ratio, peak strengthening ratio and energy absorption ratio. It is obvious that the use of CR epoxy infills has a noticeably higher contribution to the peak strengthening, yield strengthening and energy absorption ratios in all samples compared to the effect of the CM grout. In addition, lower ductility exists in samples infilled by the CR epoxy for both full and 1/3 radius defects, whilst a slight increase in ductility was clear for the 2/3 radius defect samples infilled by CR epoxy. The comparison also indicates that employment of GFRP wrapping system with high strength infills (i.e CR infill) can provide higher structural efficiency in terms of peak strength and energy absorptions capabilities. The ductility, however, slightly reduced when CR infill was used and this is expected due to the increased brittleness as discussed earlier.

5. Finite element modelling (FEM)

Understanding the behaviour of piles rehabilitated with a novel wrapping system described above as a remediation method is necessary. Since it is not very efficient and economical to test rehabilitated timber piles with different configurations experimentally due to the limitations on materials, time and cost, a numerical analysis was adopted in this

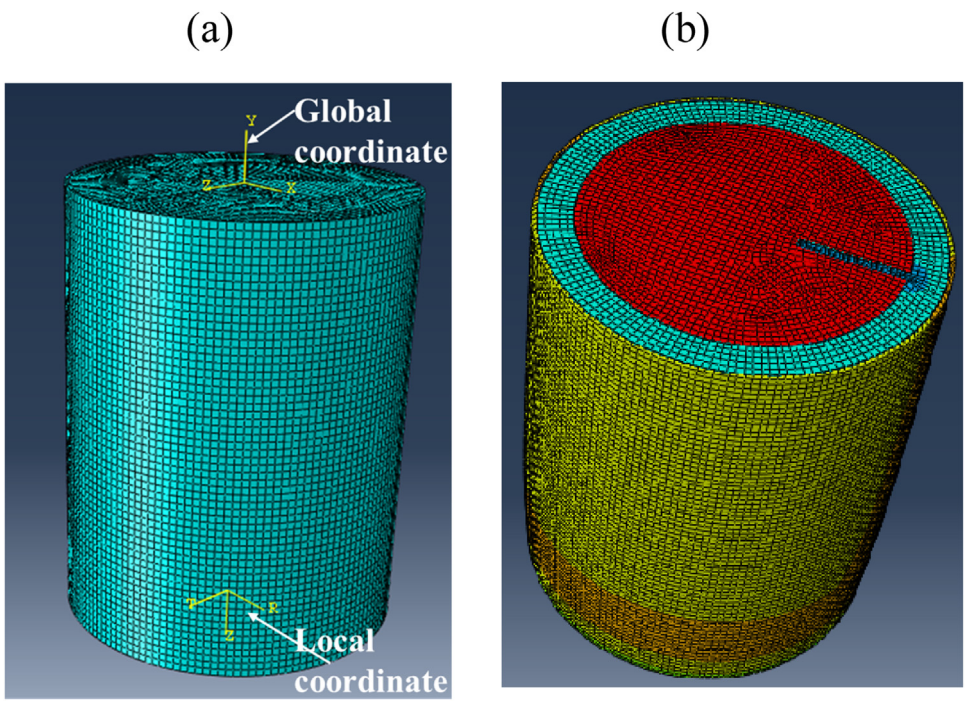

Fig. 11. Finite element model using ABAQUS: (a) FE model before analysis (b) Stress distribution of the FE model at a given time step.

Table 6
Material properties used in FEM.

Property	Timber	GFRP
Density	1100 kg/m^3	2.5E-9 kg/mm^3
Elastic modulus (E_x)	1426 MPa	21000 MPa
Elastic modulus (E_y)	2300 MPa	7000 MPa
Elastic modulus (E_z)	21078 MPa	7000 MPa
Poisson ratio (ν_{xy})	0.43	0.26
Poisson ratio (ν_{yx})	0.69	
Poisson ratio (ν_{yz})	0.043	0.3
Poisson's ratio (ν_{zy})	0.46	
Poisson's ratio (ν_{zx})	0.83	
Poisson's ratio (ν_{xz})	0.05	0.26
Shear modulus (G_{xy})		1520 MPa
Shear modulus (G_{xz})		1520 MPa
Shear modulus (G_{yz})		2650 MPa

study to achieve this broader objective. Since finite element analysis is very successful and attractive in predicting behaviour of columns, it was adopted in this study to predict the behaviour of short timber columns, which are wrapped with GFRP laminates and the annulus infilled with CR and CM infills.

5.1. Development of models

To determine the confining stresses and compare with the experimental test results, 3D finite element models were developed in ABAQUS [40]. There are 10 models to represent the different configurations used as in experimental testing program. Solid 8-node linear brick elements were used to model all different materials (timber, GFRP laminate, CR epoxy and CM grout as shown in Fig. 11. Three levels of damage due to splitting were considered in this study as explained in experimental test procedure. The split depth was introduced to the model with three different depths as described earlier by changing the geometry of the timber sample. This FEM was validated with experimental results and the validated model was used to predict the structural status of rehabilitated timber without conducting extensive experiments.

The elasto-plastic constitutive law was used to develop spotted gum timber (F27) model and orthotropic material properties was obtained from experimental tests [53], similar method was employed in [54–57]. The GFRP was modelled with linear elastic material properties. Properties for timber and GFRP are shown in Table 6. Based on the experimental tests, pin support was imposed at the bottom surface of sample and load was applied on the top surface.

Cementitious grout was modelled using isotropic material properties with a density of 2×10^6 kg/mm^3, elastic modulus of 10000 MPa and poisons ratio of 0.3. The maximum yield stress and the strain for the plastic properties for CM were assumed based on constitutive model developed by Lokuge and Aravinthan [58], manufacturer specifications and guidelines in AS 3600−2009 [59]. Crane rail epoxy was modelled with isotropic material properties with density of 2×10^6 kg/mm^3, Elastic modulus of 18000 MPa and Poisson's ratio of 0.3. The plastic properties were assumed according to the manufacturer's specifications and recommendations given by Mirza, et al. [60].

5.2. Finite element model validation

Comparisons of the experimental tests and numerical model are discussed in this section. The load versus deformation curves were plotted for each sample using the numerical model and behaviour of each sample was closely examined. The load- deformation curves compared with the experimental results for control samples, samples wrapped with cementitious grout and crane rail epoxy are shown in Figs. 12–14. The figures show that load deformation curves obtained from numerical model are closely correlated with those of the experiment results. As shown in Fig. 12, FEM simulations curves and experimental load deformation curves are in agreement in terms of the stiffness. As expected numerical results are showing reduced capacity when the defect level is higher. However, the experimental results for 1/3 radius splitting are the only outlier here and the reason is the obvious knot in the sample as shown in Fig. 12. Figs. 13 and 14 shows the comparison of force verse deformation relationship of the samples with CM and CR as the infill material in the annulus between the timber sample and the GFRP wrapping. These figures illustrate that the FEM simulations are in general agreement with the experimental curves in terms of stiffness and the general shape. However, there are some instances such as one sample for CR with 2/3 radius splitting which shows a much reduced capacity because it was failed due to the debonding of the GFRP wrapping.

Although the FEM analysis is capable of predicting the load deformation curves with a reasonable accuracy, it is a computational time extensive task which would not suit a practitioner. Hence, an analytical analysis is proposed in the following section and compared with the experimental results in the next section.

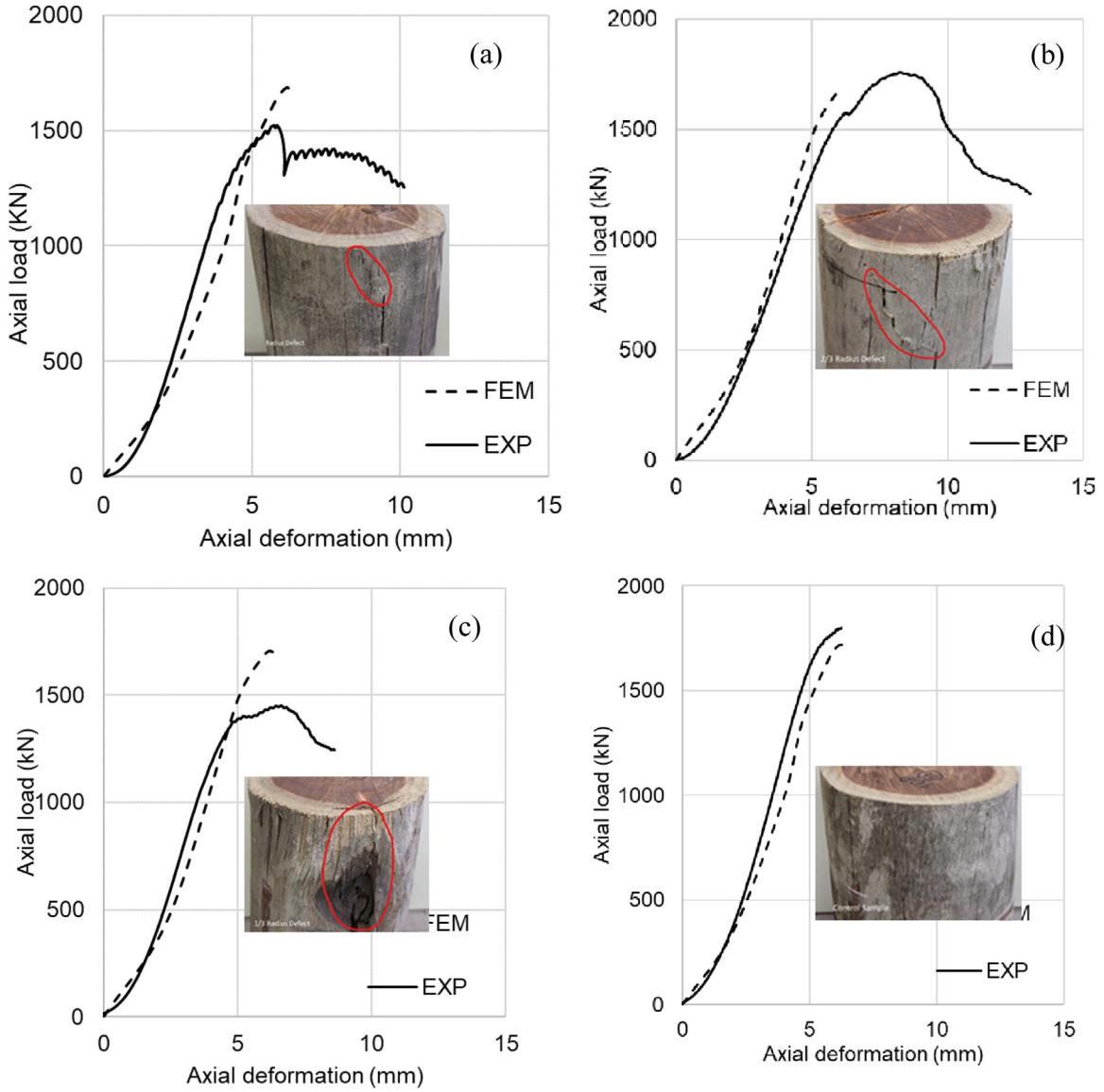

Fig. 12. Experimental and FEM model comparison of control samples: a) full radius splitting; b) 2/3 radius splitting; c) 1/3 radius splitting; d) no defect.

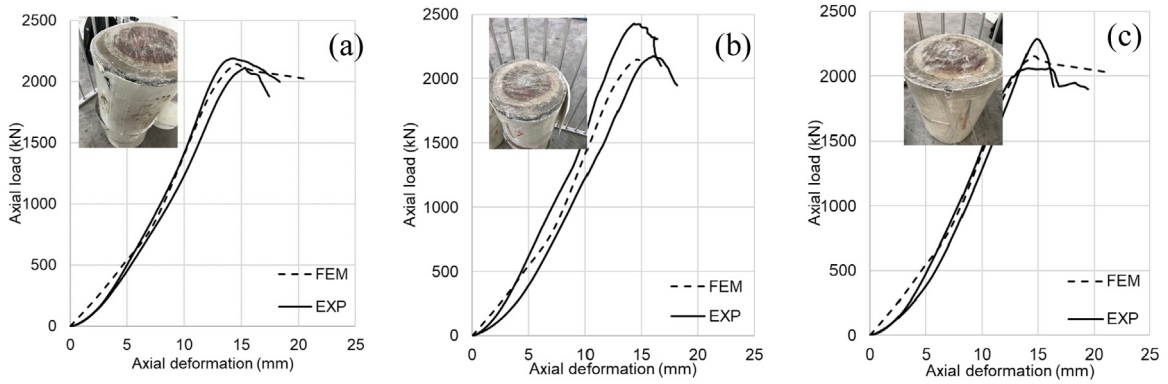

Fig. 13. Experimental and FEM model comparison of samples infilled by CM grout: a) full radius splitting; b) 2/3 radius splitting; c) 1/3 radius splitting.

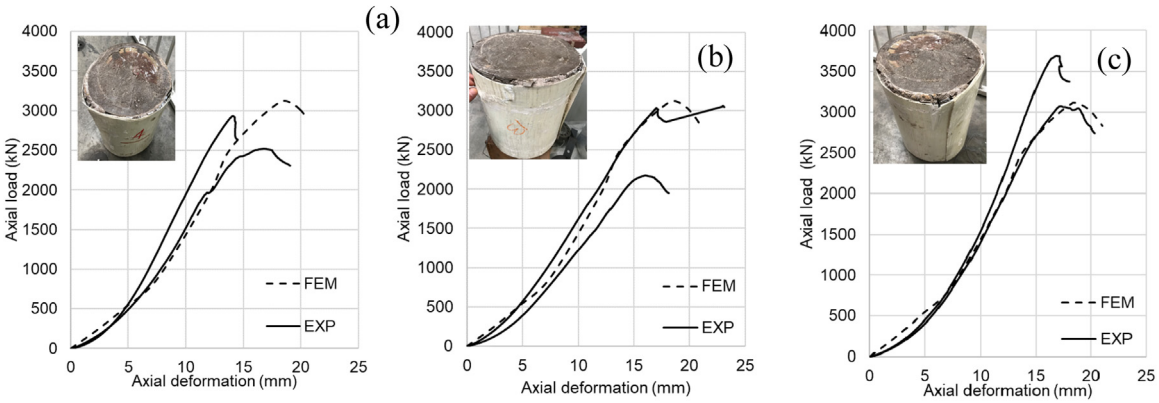

Fig. 14. Experimental and FEM model comparison of samples infilled by CR epoxy: a) full radius splitting; b) 2/3 radius splitting; c) 1/3 radius splitting.

Table 7
Confining pressures and peak stresses of GFRP wrapped infills.

Sample	A $_{timber}$ (mm^2)	A $_{defect}$ (mm^2)	A $_{effective}$ (mm^2)	A $_{infill}$ (mm^2)	f_l (MPa)	f'_c (MPa)
U-F	27806	470	27336	–	–	–
U-2/3	25413	300	25113	–	–	–
U-1/3	28659	160	28499	–	–	–
U-0	30356	0	30356	–	–	–
W-F-CM-1	26781	460	26321	15451	3.71	55.7
W-F-CM-2	27525	470	27055	15645	3.67	55.6
W-2/3-CM-1	27995	315	27680	15605	3.65	55.6
W-2/3-CM-2	31597	335	31262	16474	3.47	55.2
W-1/3-CM-1	29235	160	29075	15748	3.59	55.5
W-1/3-CM-2	29477	160	29317	15806	3.57	55.4
W-F-CR-1	27151	465	26686	15548	3.69	115.4
W-F-CR-2	28089	475	27614	15313	3.64	115.3
W-2/3-CR-1	34678	350	34328	16828	3.35	114.7
W-2/3-CR-2	29623	325	29298	15680	3.57	115.1
W-1/3-CR-1	33480	170	33310	16564	3.39	114.8
W-1/3-CR-2	34363	175	34188	16759	3.36	114.7

6. Analytical evaluation of timber column behaviour

The following section describes a simplified analytical prediction to compare the axial load capacities with the experimental results. In this prediction, the contribution of timber and the infill materials has been taken separately.

6.1. Axial- load capacity of timber core

According to AS 1720.1–2010 [43], the load capacity of timber columns is calculated by using Eq. (1).

$$N_t = \emptyset k_1 k_4 k_6 k_{12} f'_c A_c \quad (1)$$

where; N_t = Design action effect in compression, $\emptyset$ is the capacity reduction factor, k_1, k_4, k_6 *and* k_{12} are modification factors, f'_c is the characteristic value in compression parallel to grain and A_c is the cross-sectional area of timber column. The modification factors were set to 1.0 as nominal load capacities are considered in this analysis. The effective timber cross-sectional area was calculated as the total timber cross sectional area minus the defect area and results are listed in Table 7. The stress in timber was assumed to have reached its peak stress (51 MPa) in accordance with [43] as the strength parallel to grain for F27 grade timber.

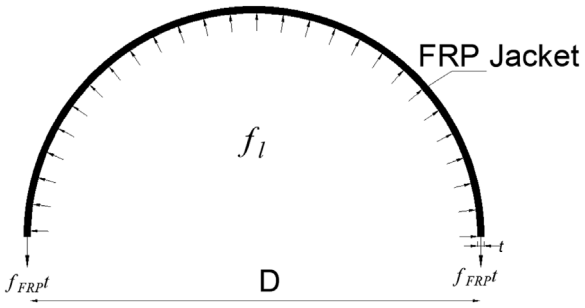

Fig. 15. Confinement effect of GFRP jacket.

Table 8
Comparison between analytical and experimental results for all samples.

Sample	N_t (kN)	N_f (kN)	N_{theory} (kN)	N_{exp} (kN)	N_{exp}/N_{theory}
U-F	1394	–	1394	1523	1.09
U-2/3	1281	–	1281	1760	1.37
U-1/3	1453	–	1453	1451	1.00
U-0	1548	–	1548	1800	1.16
W-F-CM-1	1342	861	2203	2216	1.01
W-F-CM-2	1380	871	2250	2191	0.97
W-2/3-CM-1	1412	868	2279	2176	0.95
W-2/3-CM-2	1594	910	2505	2428	0.97
W-1/3-CM-1	1483	874	2356	2289	0.97
W-1/3-CM-2	1495	876	2372	2059	0.87
W-F-CR-1	1361	1794	3155	2933	0.93
W-F-CR-2	1408	1765	3174	2520	0.79
W-2/3-CR-1	1751	1930	3681	2177	0.59
W-2/3-CR-2	1494	1805	3299	3033	0.92
W-1/3-CR-1	1699	1901	3600	3074	0.85
W-1/3-CR-2	1744	1923	3666	3689	1.01

6.2. Axial load capacity of GFRP wrapped infill

In any GFRP wrapped sections, the lateral pressure (f_l) provided by the GFRP jacket can be assumed to be uniformly distributed around the circumference as shown in Fig. 15. The lateral confining pressure is calculated according to Eq. (2).

$$f_l = \frac{2f_{frp}t}{D} \tag{2}$$

where, f_l = Confined pressure of GFRP jacket, f_{frp} is the tensile strength of GFRP in the transverse direction, t is the total thickness of the GFRP, and D is the inner diameter of the GFRP wrapped section. Various peak strength models were attempted in this study to predict the load carrying capacity of the GFRP wrapped sections and the expression proposed by Lam and Teng [30] was used to calculate the GFRP wrapped peak stress of infill materials as shown in Eq. (3).

$$\frac{f'_c}{f'_o} = 1 + 2\frac{f_l}{f'_o} \tag{3}$$

where f'_o and f'_c are the unwrapped and GFRP wrapped peak stresses, respectively.

The load carrying capacity of the wrapped infill (N_f) was then calculated by multiplying the GFRP wrapped peak stress by the infill cross sectional area. The values of the confining pressures and GFRP wrapped stresses provided by infills are presented in Table 7.

A comparison between the analytical (N_{theory}) and the experimental (N_{exp}) total load capacities is presented in Table 8. The analytical total load capacity was calculated as the summation of the load carrying capacities of the timber (N_t) and the GFRP wrapped infill (N_f). According to N_{exp}/N_{theory}, there is a good agreement between the experimental results and analytical predictions. Samples U-2/3 and W-2/3-CR-1, however, did not have well correlation with experimental results and this is referred to that these samples in particular, achieved unexpected experimental peak load results. Apart from the aforementioned fairly correlation, all other predictions had a difference of less than 21 % between the experimental and analytical results.

7. Conclusions

An innovative technique is proposed to rehabilitate deteriorated timber columns with deterioration mechanism as splitting. The technique considered wrapping the timber columns by GFRP laminate with annulus infilled by two types of grouts, the CM and CR infills. The behaviour of deteriorated timber columns rehabilitated with GFRP wrapping system was investigated. All samples were tested under axial compression loading and load-deformation responses were obtained. In addition, strengthening ratios, ductility factors and energy absorptions were calculated and compared. Based on the results of this study, the following conclusions are drawn:

- The degree of splitting defect in timber columns can significantly affect the axial loading capacities, ductility and energy absorption.
- The presence of crane rail epoxy infill in the GFRP wrapping system was more influencing than the underwater cementitious grout infill in enhancing the axial yield and peak loads. The highest contribution in yield and peak strengthening ratios were 238 % and 214 %, respectively for samples with epoxy infill.
- The presence of underwater cementitious grout and crane rail epoxy infills in the GFRP wrapping system effectively contributed to the energy absorption of the wrapped samples with highest contribution obtained for the epoxy infills. The highest average enhancement in energy absorption was 263 % in the GFRP wrapped 1/3 defect samples with epoxy infill. However, the ductility factors reduce as the compressive strength of the infill increases.
- The numerical FEM results using ABAQUS showed a good correlation with experimental results. Also, the analytical predictions of the total axial load capacities based on timber section capacity and confinement effect of the infill materials showed a good agreement with the experimental results.
- Although FEM validates the experimental results, the analytical method proposed using Australian standards together with available stress strain model for GFRP wrapped concrete is proven to be giving reliable results. This analytical method can be adopted by practising engineers in strengthening deteriorated timber columns.

Declaration of Competing Interest

The authors declare that they have no known competing financial interests or personal relationships that could have appeared to influence the work reported in this paper.

Acknowledgments

The authors gratefully acknowledge QuakeWrap, Inc. Australia for providing the materials and technical support while conducting this study. Assistance provided by the technical staff in P11 lab, University of Southern Queensland and Banyo Pilot Plant Precinct, Queensland University of Technology is greatly appreciated.

References

[1] W. Lokuge, N. Gamage, S. Setunge, Fault tree analysis method for deterioration of timber bridges using an Australian case study, Built Environ. Proj. Asset Manag. vol. 6 (3) (2016) 332–344.
[2] A. Mohammadi, J.H. Gull, R. Taghinezhad, A. Azizinamini, Assessment and Evaluation of Timber Piles Used in Nebraska for Retrofit and Rating, Department of Civil and Enviromental Engineering, Florida International University, Miami, Florida, 2014.
[3] Mainroads, Detalied Visual Bridge Inspection Guidlines for Timber Bridges, Main roads, Western Australia, 2014.
[4] K.R. Bootle, Wood in Australia. Types, Properties and Uses, McGraw-Hill Book Company, 1983.
[5] Austroads, Guide to Bridge Technology Part 7: Maintenance and Management of Existing Bridges, Austroads, Sydney, Australia, 2009.
[6] MainRoads-Queensland, Bridge Inspection Manual, Department of Main Raods, Queensland, 2004.
[7] W. Lokuge, M. Wilson, H. Tran, S. Setunge, Predicting the probability of failure of timber bridges using fault tree analysis, Struct. Infrastruct. Eng. 15 (6) (2019) 783–797.
[8] R.R. Avent, Durability of posted and epoxy-grouted timber piles, J. Struct. Eng. 115 (4) (1989) 826–833.
[9] R. Lopez-Anido, A.P. Michael, T. Sandford, B. Goodell, Repair of wood piles using prefabricated fiber-reinforced polymer composite shells, J. Perform. Constr. Facil. 19 (1) (2005) 78–87.
[10] W. Cui, D. Fernando, M. Heitzmann, J.M. Gattas, Manufacture and structural performance of modular hybrid FRP-timber thin-walled columns, Compos. Struct. 260 (2021) 113506.
[11] A. Bashandy, A. El-Habashi, A. Dewedar, Repair and strengthening of timber cantilever beams Wood Mater, Sci. Eng. (2018).
[12] W. Chang, Repair and reinforcement of timber columns and shear walls – a review, Constr. Build. Mater. 97 (2015) 14–24 10/30/ 2015.
[13] W. Lokuge, W. Karunasena, Ductility enhancement of geopolymer concrete columns using fibre-reinforced polymer confinement, J. Compos. Mater. 50 (14) (2015) 1887–1896.
[14] K. Rodsin, Q. Hussain, S. Suparp, A. Nawaz, Compressive behavior of extremely low strength concrete confined with low-cost glass FRP composites, Case Stud. Constr. Mater. vol. 13 (2020) e00452.
[15] A. Alsaad, G. Hassan, Utilization of CFRP for strengthening RC columns in marine environment, Case Stud. Constr. Mater. 7 (2017) 30–35.
[16] J.H. Gull, A. Mohammadi, R. Taghinezhad, A. Azizinamini, Experimental Evaluation of Repair Options for Timber Piles, Transp. Res. Rec.: J. Transp. Res. Board 2481 (1) (2015) 124–131.
[17] M.W. Hagos, Repair of Heavily Decayed Timber Piles Using Glass Fiber Reinforced Polymer (GFRP) and Cementitious Grout master of science, Department of Civil and Geological Engineering University of Manitoba, 2001.
[18] K.-H.E. Kim, B. Andrawes, Compression behavior of FRP strengthened bridge timber piles subjected to accelerated aging, Constr. Build. Mater. 124 (2016) 177–185.

[19] P. Caiza, M. Shin, B. Andrawes, Flexure-compression testing of bridge timber piles retrofitted with fiber reinforced polymers, Open J. Civ. Eng. 02 (3) (2012) 115–124.
[20] R. Lopez-Anido, A.P. Michael, T.C. Sandford, Experimental characterization of FRP composite-wood pile structural response by bending tests, Mar. Struct. 16 (4) (2003) 257–274.
[21] T.G. Ghazijahani, H. Jiao, D. Holloway, Concrete-filled circular steel tubes with a timber infill under axial compression, J. Struct. Eng. 143 (7) (2017) p. 04017037.
[22] W. Raongjant, J. Meng, Comparison experimental study on retrofitting methods of partially damaged timber columns (in English), Mater. Sci. Forum 976 (2020) 173–179.
[23] P. Wei, B.J. Wang, H. Li, L. Wang, S. Peng, L. Zhang, A comparative study of compression behaviors of cross-laminated timber and glued-laminated timber columns, Constr. Build. Mater. 222 (2019) 86–95.
[24] O. Chaallal, M. Shahawy, M. Hassan, Performance of axially loaded short rectangular columns strengthened with carbon fiber-reinforced polymer wrapping, J. Compos. Constr. 7 (3) (2003) 200–208 08/01 2003.
[25] O. Chaallal, M. Shahawy, M. Hassan, Performance of axially loaded short rectangular columns strengthened with carbon fiber-reinforced polymer wrapping, J. Compos. Constr. 7 (2003) 200–208.
[26] C. Chastre, M.A. Silva, Monotonic axial behavior and modelling of RC circular columns confined with CFRP, Eng. Struct. 32 (8) (2010) 2268–2277.
[27] M.F. Fahmy, Z. Wu, Evaluating and proposing models of circular concrete columns confined with different FRP composites, Compos. Part B Eng. 41 (3) (2010) 199–213.
[28] Y.-F. Wu, L.-M. Wang, Unified strength model for square and circular concrete columns confined by external jacket, J. Struct. Eng. 135 (3) (2009) 253–261.
[29] Z. Yan, C. Pantelides, Fiber-reinforced polymer jacketed and shape-modified compression members: II-Model, ACI Struct. J. 103 (6) (2006) 894–903.
[30] L. Lam, J.G. Teng, Strength models for fiber-reinforced plastic-confined concrete, ASCE Struct. J. 128 (5) (2002) 612–623.
[31] L. Lam, J.G. Teng, Design-oriented stress–strain model for FRP-confined concrete, Constr. Build. Mater. 17 (6) (2003) 471–489.
[32] H. Toutanji, Stress-strain characteristics of concrete columns externally confined with advanced fiber composite sheets, Mater. J. 96 (3) (1999) 397–404.
[33] H.M. Mohamed, R. Masmoudi, Axial load capacity of concrete-filled FRP tube columns: experimental versus theoretical predictions, J. Compos. Constr. 14 (2) (2010) 231–243.
[34] Y.-f. Wang, H.-l. Wu, Size effect of concrete short columns confined with aramid FRP jackets, J. Compos. Constr. 15 (4) (2010) 535–544.
[35] H.-J. Lin, C.-T. Chen, Strength of concrete cylinder confined by composite materials, J. Reinf. Plast. Compos. 20 (18) (2001) 1577–1600.
[36] A.Z. Fam, S.H. Rizkalla, Confinement model for axially loaded concrete confined by circular fiber-reinforced polymer tubes, Struct. J. 98 (4) (2001) 451–461.
[37] J. Teng, Y. Huang, L. Lam, L. Ye, Theoretical model for fiber-reinforced polymer-confined concrete, J. Compos. Constr. 11 (2) (2007) 201–210.
[38] T. Ozbakkaloglu, J.C. Lim, T. Vincent, FRP-confined concrete in circular sections: review and assessment of stress–strain models, Eng. Struct. 49 (2013) 1068–1088.
[39] V. Tamuzs, R. Tepfers, E. Zile, O. Ladnova, Behavior of concrete cylinders confined by a carbon composite 3. Deformability and the ultimate axial strain, Mech. Compos. Mater. 42 (4) (2006) 303–314.
[40] ABAQUS, ABAQUS, Dassault Systems Simulia, Providence, RI., (2018) .
[41] Five Stars Marine, Technical Data Sheet, Cementitious Underwater Grout, (2010) . http://www.fivestarproducts.com/fileuploader/download/download/?d=0&file=custom/upload/File-1420037435.pdf.
[42] Five Stars Marine, Technical Data Sheet, Crane Rail Grout, (2018) . https://www.fivestarproducts.com/crane-rail.html.
[43] AS 1720.1-2010, Timber Structures Design Methods, Australian Standard, 2010.
[44] QuakeWrap Inc. http://www.quakewrap.com/index.php.
[45] PileMedic Llc. Technical Data Sheet, PileMedic™ PLG60.60, for Structural Strengthening of Columns and Submerged Piles https://quakewrap.com.au/wp-content/uploads/2015/07/PileMedic-eePLG60.60.pdf.
[46] QuakeBond™ 220ur, Technical Data Sheet, QuakeBond™ 220UR Underwater Resin. https://quakewrap.com.au/wp-content/uploads/2015/07/QuakeBond-220UR-Underwater-Resin.pdf.
[47] F. Lam, M. Schulte-Wrede, C. Yao, J. Gu, Moment resistance of bolted timber connections with perpendicular to grain reinforcements, Proceedings of the 10th World Conference on Timber Engineering (WCTE) (2008).
[48] Z. Li, M. He, D. Tao, M. Li, Experimental buckling performance of scrimber composite columns under axial compression, Compos. Part B Eng. 86 (2016) 203–213.
[49] J.A. Nairn, Cross laminated timber properties including effects of non-glued edges and additional cracks, Eur. J. Wood Wood Prod. 75 (6) (2017) 973–983.
[50] M.N.S. Hadi, A.H.M. Algburi, M.N. Sheikh, A.T. Carrigan, Axial and flexural behaviour of circular reinforced concrete columns strengthened with reactive powder concrete jacket and fibre reinforced polymer wrapping, Constr. Build. Mater. 172 (2018) 717–727.
[51] A. Jorissen, M. Fragiacomo, General notes on ductility in timber structures, Eng. Struct. 33 (11) (2011) 2987–2997.
[52] J. Gilfillan, S. Gilbert, G. Patrick, The use of FRP composites in enhancing the structural behavior of timber beams, J. Reinf. Plast. Compos. 22 (15) (2003) 1373–1388.
[53] R. Elsener, Material Characterization of Timber Utility Poles Using Experimental Approaches, University of Technology Sydney, 2014.
[54] S. Navaratnam, J. Thamboo, K. Poologanathan, K. Roy, P. Gatheeshgar, Finite element modelling of timber infilled steel tubular short columns under axial compression, Structures, 30, Elsevier, 2021, pp. 910–924.
[55] S. Navaratnam, N. Herath, W. Lokuge, J. Thamboo, K. Poologanathan, Performance of timber girders with end-notch: experimental and numerical investigation, Structures, vol. 29, Elsevier, 2021, pp. 730–740.
[56] N. Satheeskumar, Wind Load Sharing and Vertical Load Transfer from Roof to Wall in a Timber-framed House, James Cook University, 2016.
[57] M. Oudjene, M. Khelifa, Elasto-plastic constitutive law for wood behaviour under compressive loadings, Constr. Build. Mater. 23 (11) (2009) 3359–3366.
[58] W. Lokuge, T. Aravinthan, Stress-strain behaviour of unconfined polymer concrete, 23rd Australian Conference on the Mechanics of Structures and Materials (ACMSM23), vol. 1, Southern Cross University, Lismore, NSW, 2014, pp. 161–166.
[59] AS3600-2009, Concrete Structures, Australian Standard, Sydney, NSW, 2009.
[60] A. Mirza, N. Aziz, W. Ye, J. Nemcik, Mechanical properties of grouts at various curing times, in: Naj Aziz, Bob Kininmonth (Eds.), Proceedings of the 16th Coal Operators' Conference, Mining Engineering, University of Wollongong, 10-12, February 2016, 2016 no. 10-12 February 2016, pp. 84-90.